Automated cardiac MRI analysis for robust profiling of heart failure models in mice

Thulaciga Yoganathan[1*], Matt Sooknah[1], Baby Martin-McNulty[1], James Lee[1], Florian Schmid[1], Austin Lefebvre[1], Frank Kober[2], Johannes Riegler[1*]

[1]Calico Life Sciences LLC, 1170 Veterans Blvd, South San Francisco, CA 94080, USA

[2]Aix-Marseille Univ, CNRS, Centre de Résonance Magnétique Biologique et Médicale (CRMBM), Marseille, France

[*] Corresponding authors

Supplementary Information

Supplementary Table

Supplementary Table S1

SAx cine scans	SF	SF40	MB	IG
Echo Time (ms)	1.8	1.8	1.8	2.8
Repetition Time (ms)	5-6	5-6	5-6	6.209
Flip Angle (degrees)	15	15	15	15
Dummy scans	10	10	10	388
Dummy scan duration (ms)	1191.937	1191.937	50	2409.194
Oversampling	---	---	---	60
Frames	20	20	20	20
ECG and Respiratory double gating	Yes	Yes	Yes	No
Navigator signal	---	---	---	in-slice
Slice thickness (mm)	0.8	0.8	0.8	0.8
Number of slices of a scans stack	12	12	12	12
Field of view (mm)	25x25	25x25	25x25	25x25
Matrix size	192x192	192x192	192x192	192x192
Resolution (mm)	0.130x0.130 mm	0.130x0.130 mm	0.130x0.130 mm	0.130x0.130 mm
Number of averages	1	1	1	1
Percent sampling along phase encoding direction	100	60	100	100
Flow compensation	Yes	Yes	not implemented	not implemented
Bandwidth (Hz)	74k	74k	74k	74k
Anti-aliasing	1x1	1x1	1x1	1x1
Scan duration of the whole stack (minutes)	10	7	7	15

Supplementary Table S1: Table detailing cardiac MRI acquisition parameters for four different short-axis sequences.

Supplementary Figures

Supplementary Figure S1

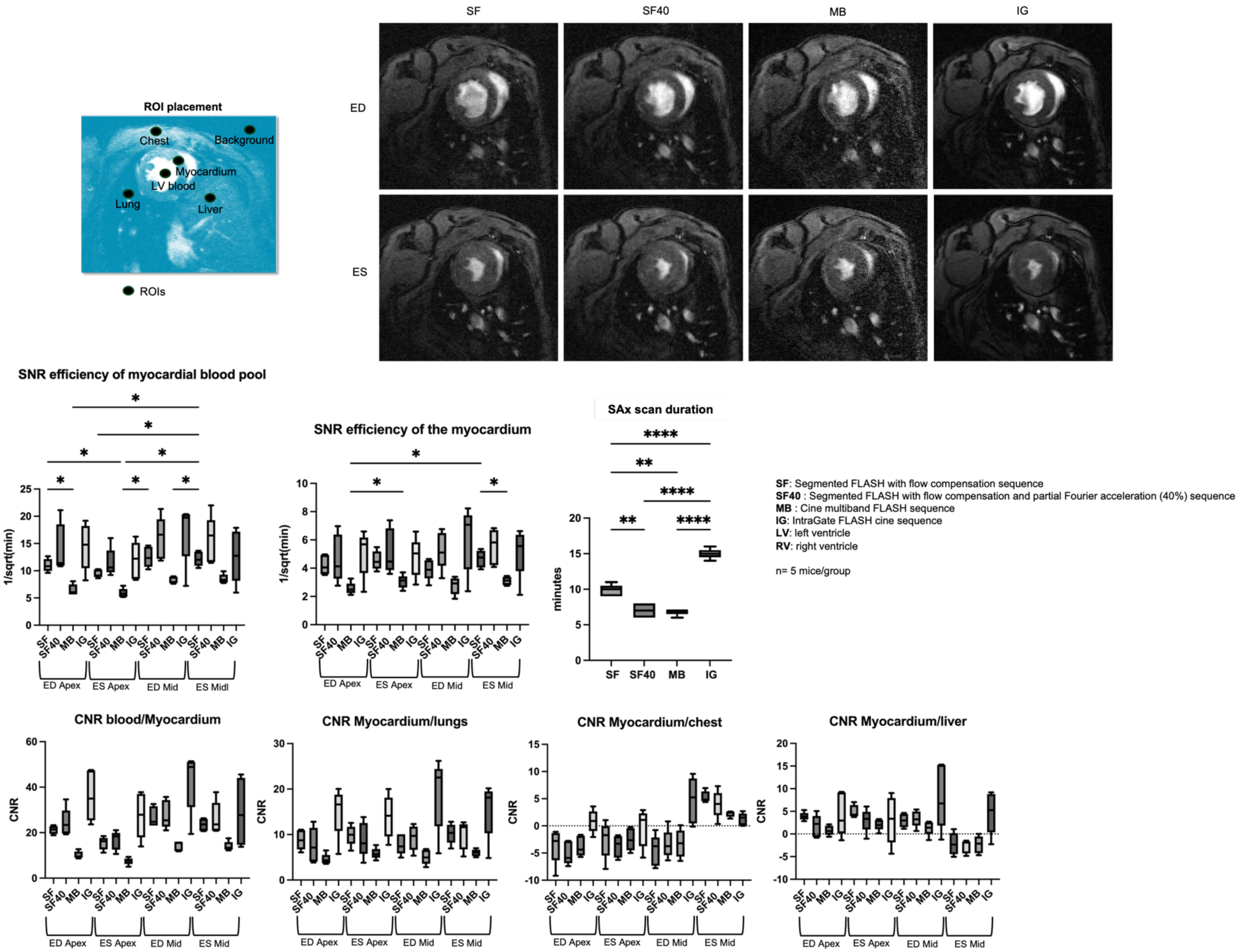

Supplementary Figure S1. Evaluation of short-axis cine MRI sequences in healthy mice

Comparison of four different short-axis cine MRI sequences: segmented FLASH without (SF) or with (SF40) partial Fourier acceleration, simultaneous multiband FLASH (MB), and IntraGate FLASH (IG). The graphs display the signal-to-noise ratio (SNR) efficiency and contrast-to-noise ratio (CNR) for each sequence, demonstrating the trade-off between image quality and acquisition time (n=6 per group). While the IG sequence exhibits the highest SNR efficiency and CNR, its significantly longer scan time makes it less suitable for comprehensive cardiac imaging in mice. The SF40 sequence offers a favorable balance between image quality and acquisition time, making it a good option for our preclinical cardiac MRI studies.

Supplementary Figure S3

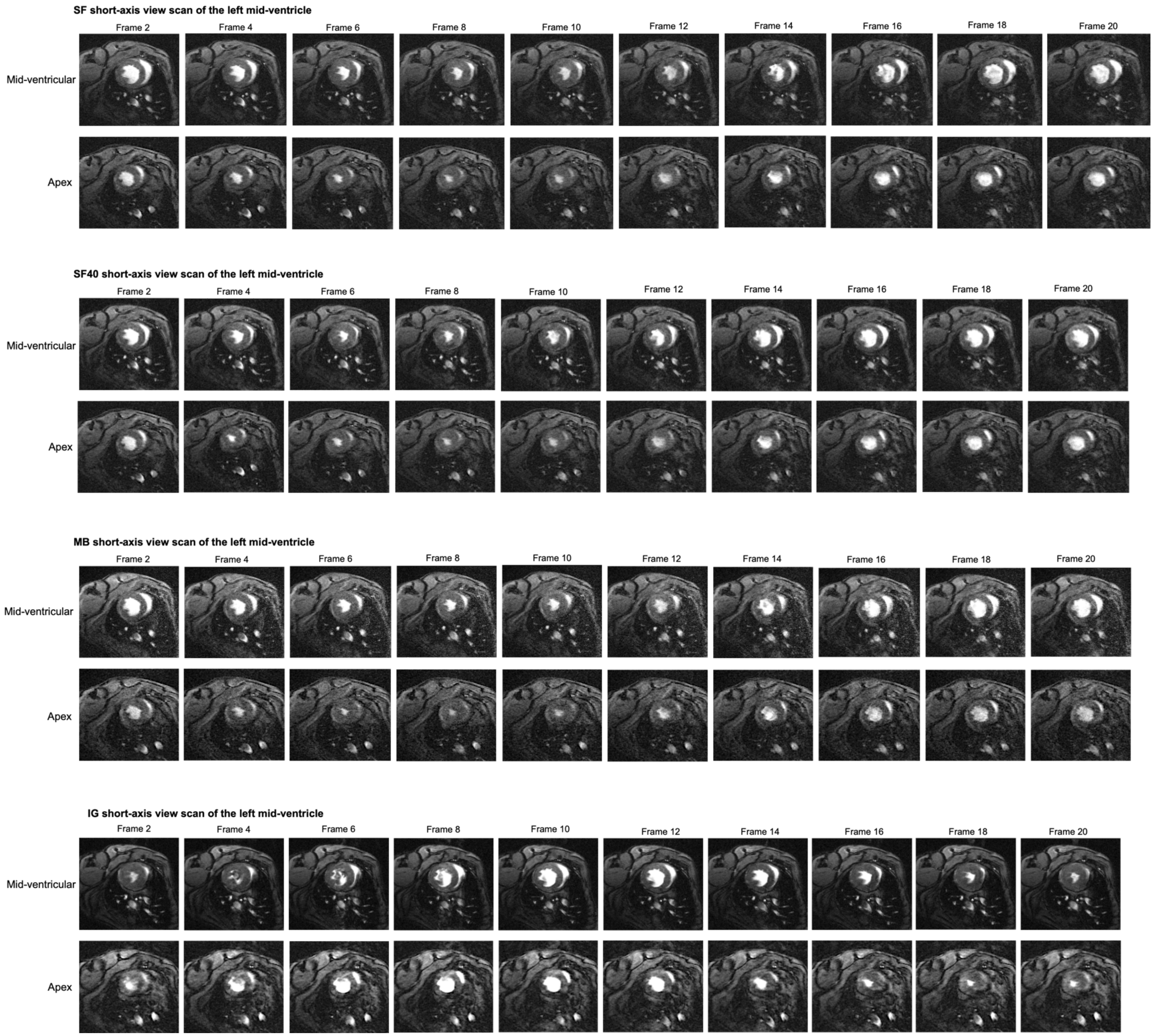

Supplementary Figure S2: Representation of the mid-ventricular and apical slices' frames of the four short-axis view sequences performed in healthy female mouse.

Supplementary Figure S3

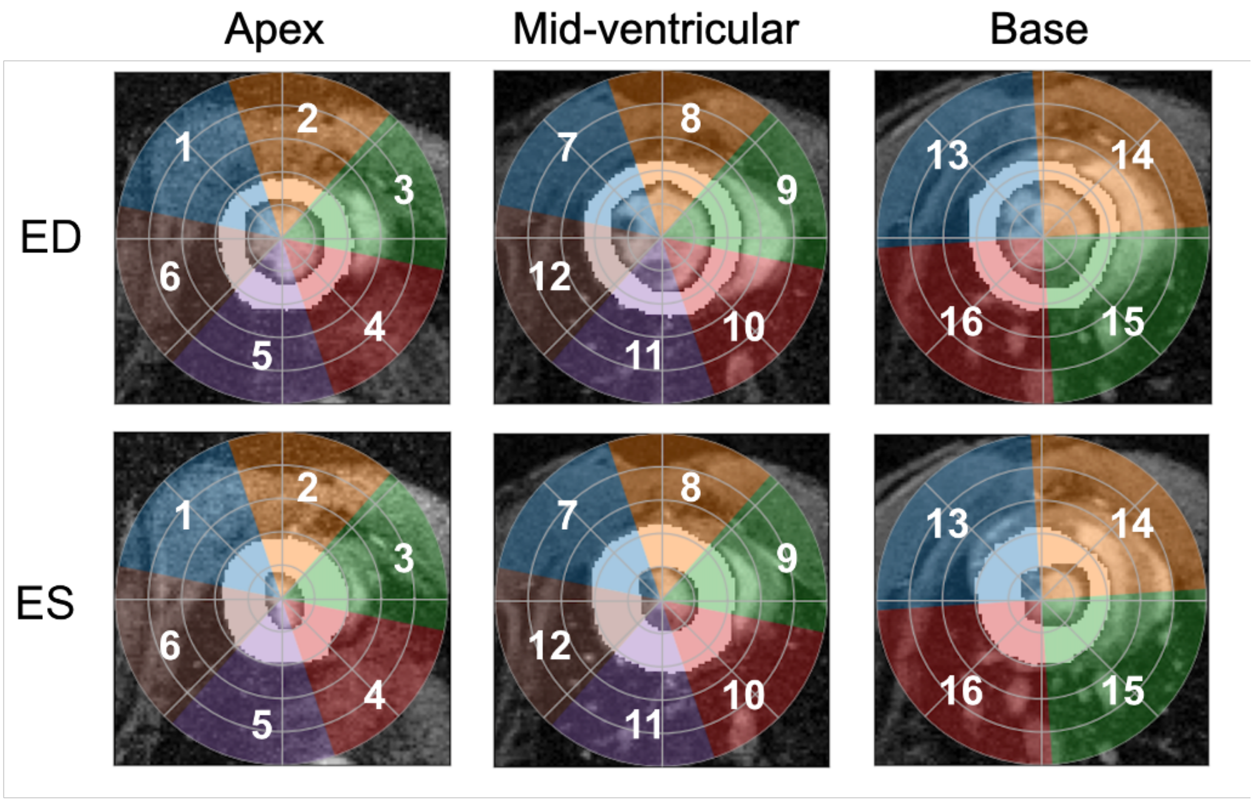

Supplementary Figure S3: Deep learning based left ventricular wall thickness' segmentation. The wall is divided into 17 segments.

Supplementary Figure S4

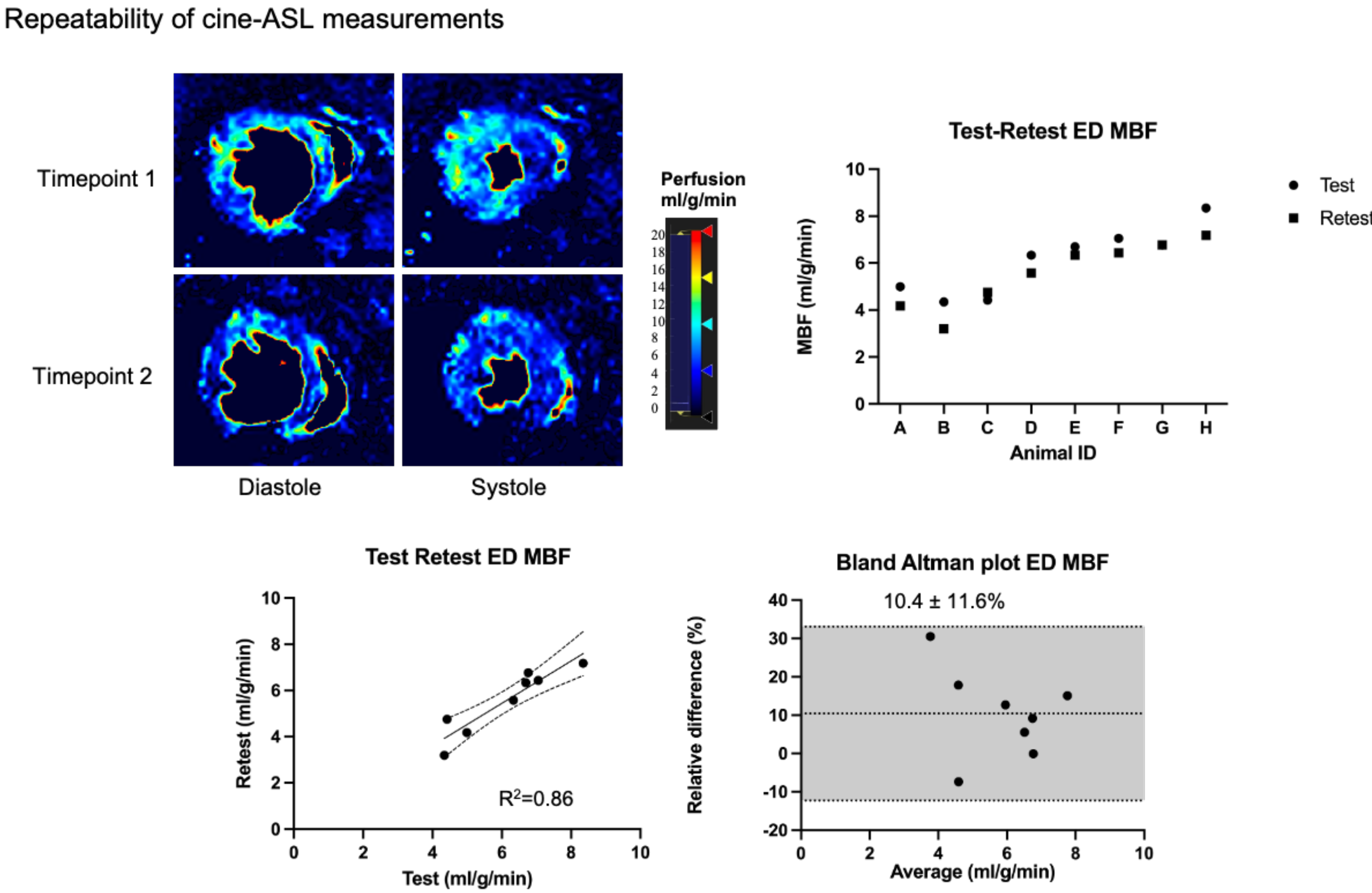

Supplementary Figure S4: Validation of cine-ASL myocardial perfusion quantification

Representative cine-ASL myocardial perfusion maps in a healthy mouse heart at different time points at LV end-diastole and end-systole. The color scale represents myocardial blood flow (MBF) in ml/g/min. Bland-Altman plot showing good agreement between repeated cine-ASL measurements. The plot displays the difference between the two measurements against the mean of the two measurements. The solid line represents the mean difference, and the dashed lines represent the 95% limits of agreement. Scatter plot demonstrating the strong correlation (r = 0.86) between repeated cine-ASL measurements of MBF in healthy mice (n=8).

Supplementary Figure S5

Intra-class correlation coefficient (ICC) to assess the reliability of the CNN-segmentation method

	EDV J vs T	ESV J vs T	SV J vs T	LVEF J vs T	RVEF J vs T	wED J vs T	wES J vs T	FS J vs T
ICC_3	**0.96**	**0.95**	**0.92**	**0.89**	**0.62**	**0.85**	**0.64**	**0.70**

	EDV J vs ML	ESV J vs ML	SV J vs ML	LVEF J vs ML	RVEF J vs ML
ICC_3	**0.99**	**0.99**	**0.97**	**0.97**	**0.77**

	EDV T vs ML	ESV T vs ML	SV T vs ML	LVEF T vs ML	RVEF T vs ML
ICC_3	**0.97**	**0.98**	**0.94**	**0.93**	**0.70**

	ASL test-retest healthy heart
ICC_1	**0.86**

Bland-Altman to assess the reliability of the CNN-segmentation method vs. observers

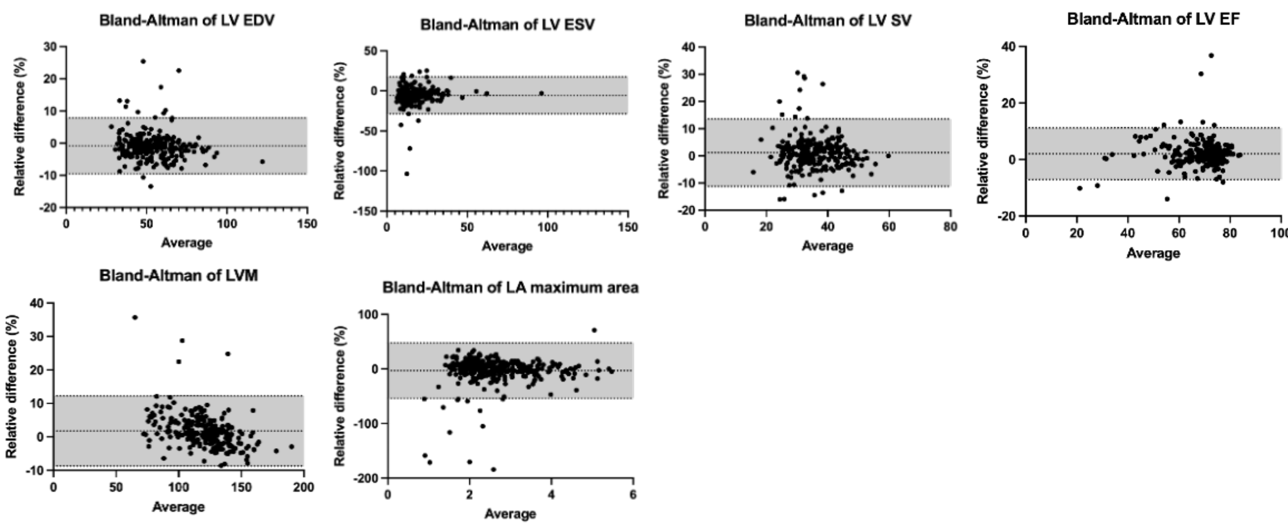

Supplementary Figure S5: Tables of intra-class correlation coefficients and Bland-Altman analysis to assess the reliability of the CNN-segmentation method (ML) against manual segmentation (observers J and T) suggest high agreement between CNN and manual segmentations.

Supplementary Figure S6

Preserved blood pressure and left ventricular function in DIO mice

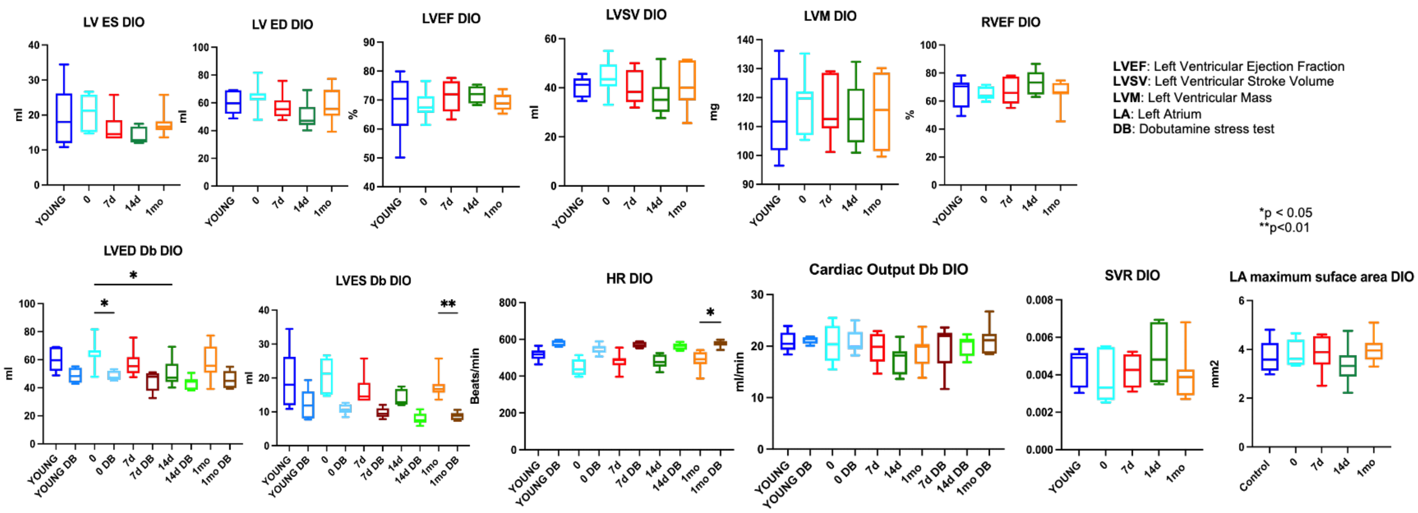

Left ventricular function indexed to mouse body weight and LV wall thickness in DIO+DOCP mice

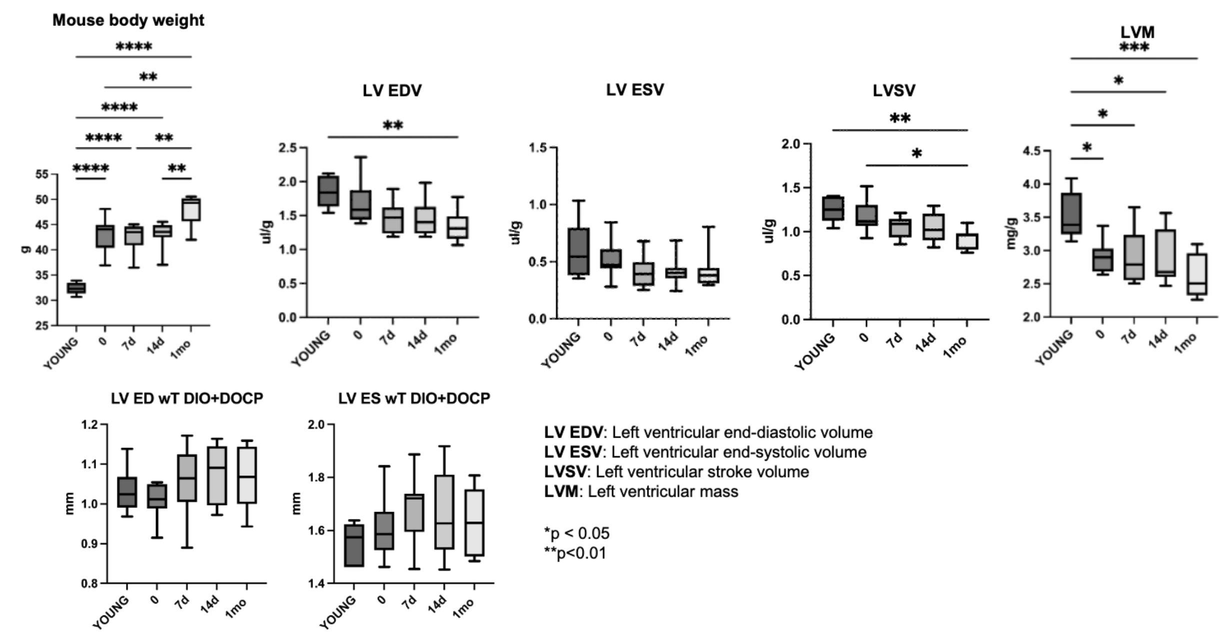

Impaired myocardial blood flow (MBF) in DIO and DIO DOCP mice

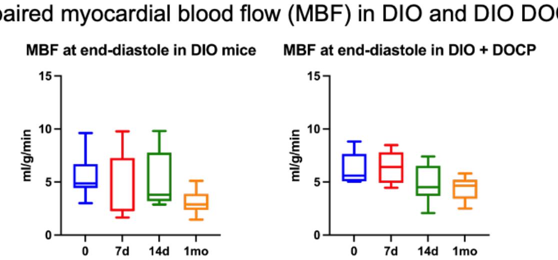

Supplementary Figure S6: cardiac MRI-derived LV and RV functional parameters assessment in DIO and DIO+DOCP groups.

Supplementary Figure S7

Left ventricular function indexed to mouse body weight and LV wall thickness in middle-aged HFD+DOCP mice

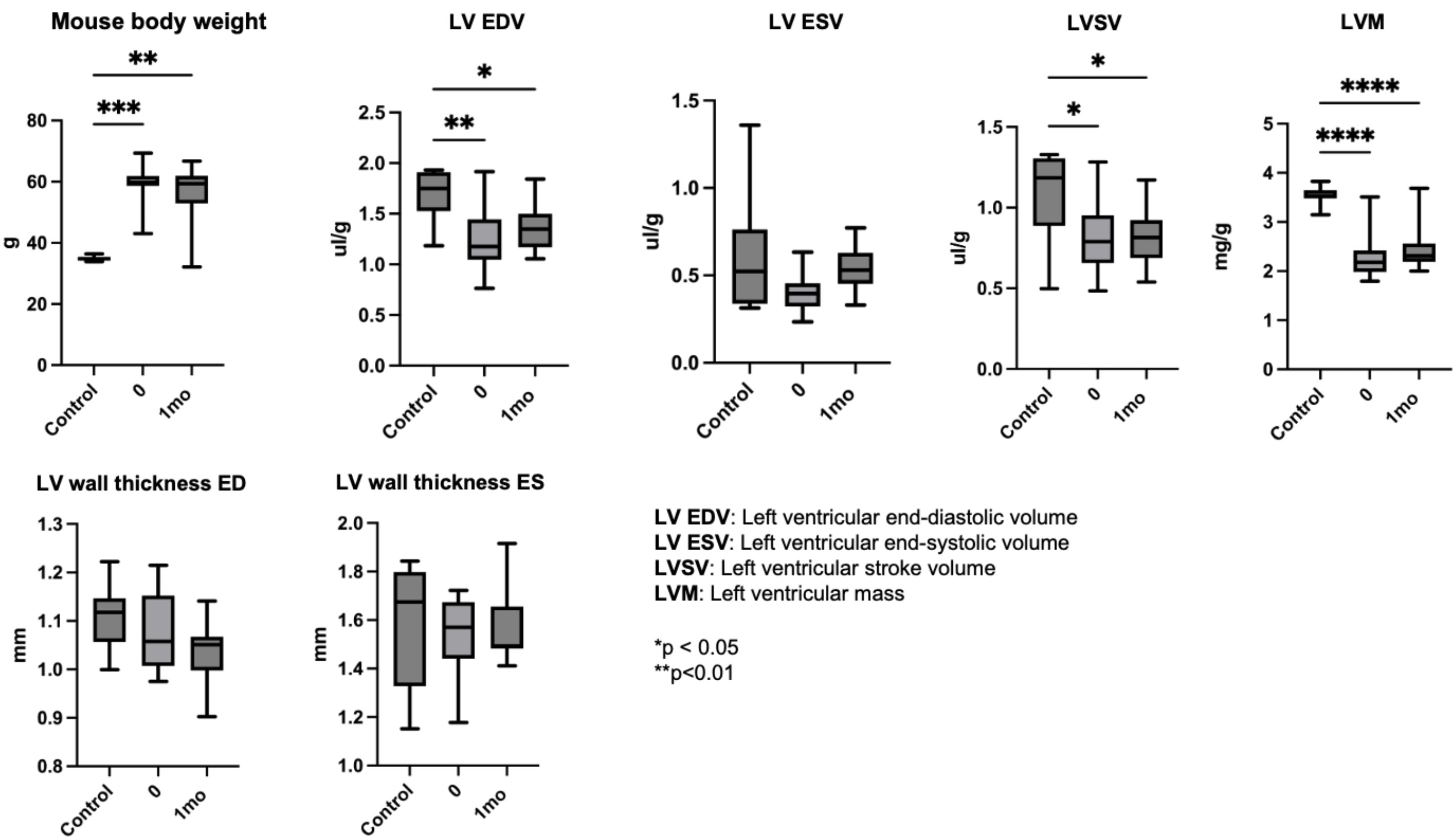

Supplementary Figure S7: Cardiac MRI-derived LV functional parameters indexed to mouse body weight.

Supplementary Figure S8

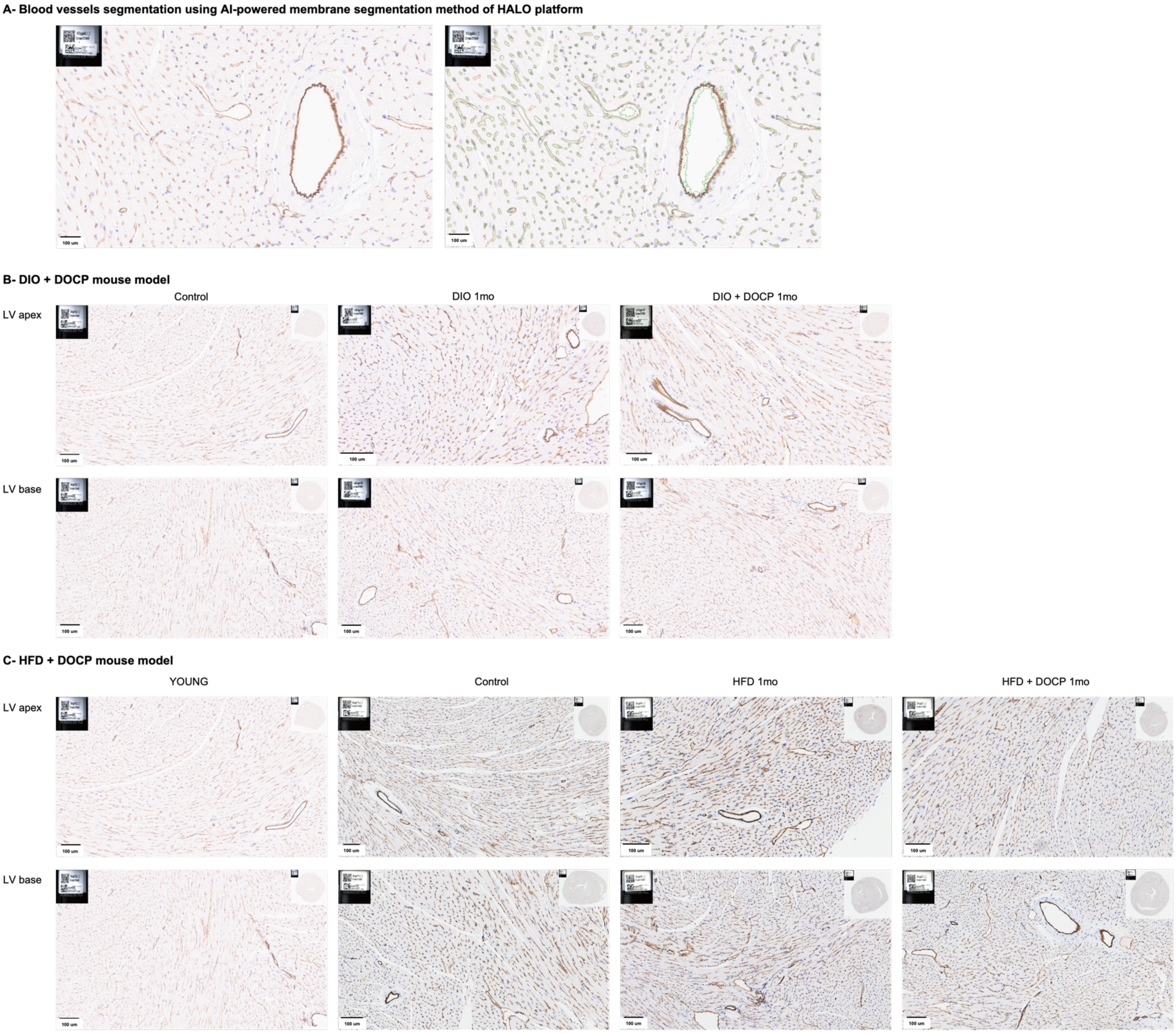

Supplementary Figure S8: Assessment of microvascular density in cardiac tissue using CD31 HIC staining and automated image analysis in green (A) in DIO+DOCP (B) and HFD+DOCP (C) mouse models.